Electrochemically Deposited Ceria Structures for Advanced Solid Oxide Fuel Cells

Thesis by

Evan C. Brown

In Partial Fulfillment of the Requirements

For the Degree of

Doctor of Philosophy

California Institute of Technology

Pasadena, California

2011

(Defended May 20, 2011)

Acknowledgements

Foremost, I would like to dedicate this work to the One who loved me first. Truly, there is no greater love than one who lays down his life for another.

I would like to thank my wife for giving me such support and encouragement. Those words are easily written, but they were never given lightly by her. As for the rest of my family, I would not have accomplished much without all of their love and their crazy; especially my parents, who inspire me and have always reminded me who I am.

I also want to thank Sossina Haile for being my advisor and my advocate—without her help, this manuscript would be 100 times longer with half as much insight. She has shown me how compassion and strength can blend together in true leadership. And I want to thank my labmates and science friends for the community and fellowship we have shared. Particularly, I want to thank Dr. William Chueh for too many things to count (but specifically for analysis, measurements, and insights pertaining to Chapter 4), Dr. Yong Hao (Chapter 4, microfabrication), Dr. David Boyd for his analytical expertise, and Stephen Wilke (Chapter 2, fabrication and SEM assistance). Also, to Taesik Oh, Aron Varga, Mary Louie, Carol Garland (TEM), Jane Liu (FIB), Aminy Ostfeld, and Sylvia Sullivan for invaluable discussions and technical assistance. I would also like to acknowledge the Global Climate and Energy Program in conjunction with Stanford University for funding.

Abstract

As the pursuit towards emissions reduction intensifies with growing interest and nascent technologies, solid oxide fuel cells (SOFCs) remain an illustrious candidate for achieving our goals. Despite myriad advantages, SOFCs are still too costly for widespread deployment, even as unprecedented materials developments have recently emerged. This suggests that, in addition to informed materials selection, the necessary power output—and, thereby, cost-savings—gains must come from the fuel cell architecture. The work presented in this manuscript primarily investigates cathodic electrochemical deposition (CELD) as a scalable micro-/nanoscale fabrication tool for engineering ceria-based components in a SOFC assembly. Also, polymer sphere lithography was utilized to deposit fully connected, yet fully porous anti-dot metal films on yttira-stabilized zirconia (YSZ) with specific and knowable geometries, useful for mechanistic studies. Particular attention was given to anode structures, for which anti-dot metal films on YSZ served as composite substrates for subsequent CELD of doped ceria. By tuning the applied potential, a wide range of microstructures from high surface area coatings to planar, thin films was possible. In addition, definitive deposition was shown to occur on the electronically insulating YSZ surfaces, producing quality YSZ|ceria interfaces. These CELD ceria deposits exhibited promising electrochemical activity, as probed by A.C. Impedance Spectroscopy. In an effort to extend its usefulness as a SOFC fabrication tool, the CELD of ceria directly onto common SOFC cathode materials without a metallic phase was developed, as well as templated deposition schemes producing ceria nanowires and inverse opals.

Table of Contents

List of Figures

List of Tables

List of Symbols and Notations

n	number of electrons
F	Faraday's constant
E_N	Nernstian voltage
δ	oxygen non-stoichiometry
$Ce^{3+/4+}$	dissociated aqueous cerium ions of a particular cerium valence
Ce(III/IV)	precipitated/solid cerium species of a particular cerium valence
ρ_{3PB}^{theo}	theoretical 3PB areal density
ρ_{3PB}^{exp}	experimental 3PB areal density
f_{2PB}^{theo}	theoretical 2PB area fraction
f_{2PB}^{exp}	experimental 2PB area fraction
ϕ_i	initial PS sphere diameter
ϕ_f	final PS sphere diameter
D	crystallite size
λ	XRD x-ray wavelength
β	adjusted full-width half max
θ	XRD diffracting angle
Z	complex impedance
R	resistance
C	capacitance
ω	frequency
j	$\sqrt{-1}$

$\tilde{Z}$	complex impedance normalized by total deposited area
$\tilde{R}$	resistance associated with a Nyquist arc normalized by total deposited area
$\tilde{Z}^*$	complex impedance normalized by the projected area of the exposed SDC surface
$\tilde{R}^*$	resistance associated with a Nyquist arc normalized by the projected area of the exposed SDC surface

Abbreviations

SOFC	solid oxide fuel cell
CELD	cathodic electrochemical deposition
YSZ	yttria-stabilized zirconia
OCV	open circuit voltage
SDC	samaria-doped ceria
GDC	gadolinia-doped ceria
MIEC	mixed ionic-electronic conductor
3PB	three-phase boundary
2PB	two-phase boundary
PLD	pulsed-laser deposition
CVD	chemical vapor deposition
AELD	anodic electrochemical deposition
PS	polystyrene
SEM	scanning electron microscopy
AFM	atomic-force microscopy

HSA	high surface area
SCE	standard calomel electrode
XRD	x-ray diffraction
FT-IR	Fourier transform infrared
CV	cyclic voltammetry
EDS	x-ray energy dispersive spectroscopy
TEM	transmission electron microscopy
ACIS	A.C. impedance spectroscopy
ASR	area-specific resistance
LF	low frequency
HF	high frequency
AAO	anodic aluminum oxide
BSCF	$Ba_{0.5}Sr_{0.5}Co_{0.8}Fe_{0.2}O_{3-\delta}$
SCN	$Sr_xCo_yNb_zO_{3-\delta}$

Chapter 1
Introduction and Background

1.1 A Global Perspective

Eventually, the world will run out of fossil fuels, period. This simple fact necessarily motivates an intensive search for alternatives. As if to underscore the immediacy of such a quest, geopolitical tensions and complications have again and again proven to disrupt what people love most about fossil fuels—they are consistently available, relatively easy to use, and, above all else, cost little to do so. Finding a (host of) suitable replacement candidate(s) is difficult, owing to the plethora of pros to using fossil fuels. Indeed, societies worldwide have in many cases developed around their day-to-day use, making widespread adoption of anything else a nearly overwhelming task: humans are loathe to radically change. Nevertheless, the pioneer views this picture as ripe with opportunity, and science has historically cast itself as a trail blazer of progress.

There is a finite amount of energy that is available for power generation, in any form. And since thermodynamics dictates that energy cannot be created or destroyed, we are limited to options such as solar, wind, nuclear, hydroelectric, tidal, biomass, and geothermal forms of energy. Of these, solar energy is far and away the most abundant, and, therefore, the most practical to develop. Even as all of the so-called “renewable energy” technologies are considered, two of the most attractive, solar and wind, suffer from intermittency issues— the sun only shines during the day, and inclement weather can be prohibitive; wind is notoriously temperamental. Energy storage media are necessary to complement a system that relies solely on these renewable energy technologies for power generation. Energy that is converted from solar or wind could be used at a later time, for instance, when the electricity demand exceeds the supply ability, like at night or when the wind isn't blowing. Chemical bonds remain the most efficient energy storage method, although significant gains have been made in batteries and supercapacitors [1-4]. But once a fuel is made, there is the question of how one extracts the stored energy. Humans have almost entirely relied upon combustion of fossil fuels to do so, but the by-products invariably add to the growing amount of greenhouse gases in the earth's atmosphere. With the daunting prospect of global climate change, a better fuel (and way of extracting its stored energy) is desperately needed.

Fuel cells have tremendous promise to address these concerns. A fuel cell is an energy conversion device that relies upon electrochemical driving forces to extract energy from a fuel as electricity, rather than the familiar, but Carnot-restricted combustion cycles. This allows more of the chemical potential in a fuel to be converted into useful work, with calculated efficiencies in excess of 80% for combined heat and power systems [5]. Fuel cells operating at higher temperatures can run off of a wide range of fuels, from standard, already-in-use fossil fuels to pure hydrogen. This flexibility is a pragmatic necessity for bridging the current addiction to greenhouse-gas-producing fuel to a "clean", carbon-free source. A number of future scenarios can be imagined, but a particularly compelling vision for the power generation of the future is to utilize solar energy to split water into hydrogen and oxygen, where the hydrogen is stored until power is needed. The hydrogen could then be utilized as the fuel in a fuel cell, producing electricity. The by-product of such a process is water, which can be fed back to the original input stream.

Challenges undoubtedly remain. Chief among those are economic—fuel cells are ~10-100 times too expensive to be competitive [5-6]. To ameliorate this issue, better performing and cheaper materials/fabrication processes need to be developed.

This manuscript concentrates on combining modern, high-performance materials with advanced architectural designs of solid oxide fuel cells (SOFCs), all to achieve the ultimate goal of dramatically increasing their power output. Two fairly well-established fabrication methods with little to no prior demonstration of actual application in a fuel cell are utilized here for SOFCs, namely, polymer sphere lithography [7-8] for substrate preparation and cathodic electrochemical deposition [9-10] for oxide material deposition. Extensive modifications and further development was needed to appropriately adapt them, which are the subjects of Chapters 2 and 3. Chapter 4 details activity analyses of various SOFC components made with these fabrication methods, and Chapter 5 involves the fabrication of specialized microstructures. First, however, a broad introduction to SOFC operational basics is presented in Section 1.2, and the necessary linkage of, applicability towards, and motivation for utilizing polymer sphere lithography and cathodic electrochemical deposition in SOFC fabrication is subsequently established in sections 1.3 and 1.4, respectively.

1.2 SOFC Introduction

1.2.1 *SOFC Basics*

A fuel cell consists of three main components: an electrolyte sandwiched between two electrodes, the anode and cathode. The electrolyte is an ionically conducting material, allowing ions, but not electrons, to migrate through it. Fuel cells are typically categorized

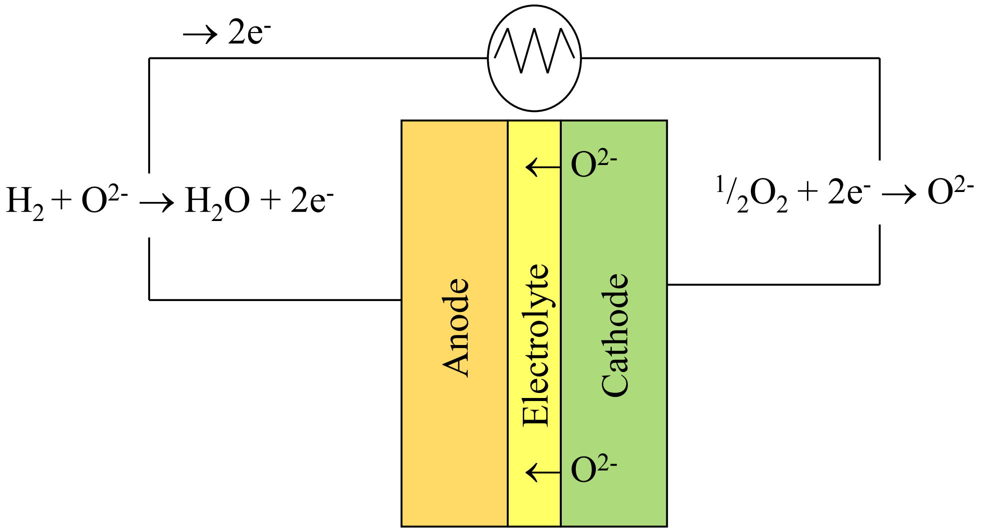

Fig. 1.1. A schematic of a generalized SOFC, showing each electrode's half-reactions and the migration directions of each mobile species.

by their mobile ionic species and temperature of operation. In this manuscript, solid oxide fuel cells are the focus. They are solid-state devices (meaning no liquid electrolytes) and typically conduct oxygen ions through metal oxide constituents, although some proton-conducting SOFCs exist [11-12]. Each electrode is responsible for facilitating transport of electrons, oxygen ions, and gaseous reactants to surface reaction sites, where the appropriate half-cell reaction occurs. A schematic of a generalized SOFC is shown in Fig. 1.1. On the anode side, fuel is introduced, where it reacts with oxygen ions supplied from the cathode that have migrated through the solid electrolyte, producing water vapor and electrons, according to the half-reaction in Eqn. 1.1.

$$H_2(g) + O^{2-} \rightarrow H_2O(g) + 2e^- \qquad (1.1)$$

Driven by the need to maintain overall charge neutrality, the negatively charged electrons travel through an externally connected circuit to the cathode, effectively offsetting the dearth of negative charge left by migrating oxygen ions. These incoming electrons then react with atmospheric oxygen, producing oxygen ions according to the half-reaction:

$$\tfrac{1}{2}O_2(g) + 2e^- \rightarrow O^{2-} \tag{1.2}$$

The two electrode half-reactions combine to yield the overall reaction given in Eqn 1.3, from which the ΔG_{rxn} can be calculated and then converted to a Nernstian voltage (Eqn. 1.4), measured as the open circuit potential (OCV), where *n* is the number of participating electrons and *F* is Faraday's constant. This is the potential at which no net current is flowing through the cell. For the high temperatures of SOFCs and pure oxygen/hydrogen atmospheres, typical OCVs are ~1.1 V.

$$H_2(g) + \tfrac{1}{2}O_2(g) \rightarrow H_2O(g) \tag{1.3}$$

$$E_N = \frac{\Delta G_{rxn}}{nF} \tag{1.4}$$

Various deleterious phenomena decrease the operating voltage from the theoretical Nernstian value, as depicted in the polarization curve of Fig. 1.2. A cell's power output is defined as the operating voltage multiplied by the drawn current, meaning that these processes lower SOFCs' power output. At open circuit conditions, leaks in the sealing that separate the anodic and cathodic compartments, as well as holes in the solid electrolyte, can allow fuel cross-over, which immediately lowers the operating voltage. Also, non-zero electronic conductivity in the solid electrolyte has the same effect. Once current is drawn from the cell, three so-called overpotentials further decrease the operating voltage. Activation overpotentials are related to the finite-rate electrode reaction kinetics, and typically dominate the voltage losses. Ohmic overpotentials originate from conductivity resistances encountered when charged species

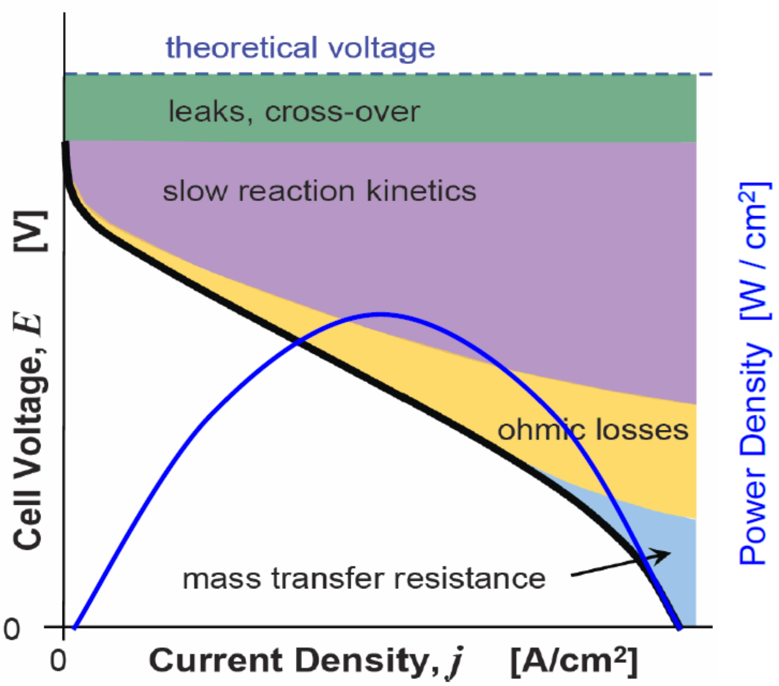

Fig. 1.2. A visualization of the overpotential losses typically encountered in SOFCs and the associated power density output of such a cell.

migrate throughout the cell. Concentration overpotentials arise when not enough reactants are supplied to the half-reaction sites, most often caused by mass transfer limitations in the gas phase, but these effects are only seen at very high current densities beyond practical operating conditions.

Species' transport through the crystal structure of metal oxides is generally thermally activated, and electrode kinetics are enhanced as temperature increases; therefore, high temperatures are desirable as they increase conductivity and reaction rates. Standard SOFC operating temperatures are anywhere from 700 – 1000 °C [5-6]. These high temperatures enforce strict requirements for component materials, even making choice of the interconnect material, which conducts the electrons to and from the respective electrodes, a complicated matter. In fact, the lack of cheap, viable options for high temperature interconnects has largely motivated the move toward intermediate operating temperatures, i.e., 500-650 °C. This is the point at which stainless steel and its derivatives can resist prohibitive oxidation, and could therefore conceivably be used for interconnects [13]. Furthermore, thermal cycling can lead to significant wear and tear due to differences in thermal coefficients of expansion, although it is less severe at lower temperatures.

Manufacturing scalability and its cost is a perpetual concern. Low-throughput, expensive fabrication processes cannot be a part of the final solution, although they can be useful toward more fundamental understanding. Similarly, catalytic materials can be used to impact and define sluggish reaction kinetic pathways, but they often consist of expensive, rare precious metals such as platinum or palladium [14]. Even though much lower operating temperatures can be achieved, this strategy is not viable on a large scale.

With so many aspects to SOFC technology, a methodical approach is needed to gain fundamental insights and elucidate the rate-limiting steps, eventually contributing to an informed, optimized design. From the brief overview above, two design focal points emerge—materials selection and cell architecture.

1.2.2 *Materials Selection: Samaria-Doped Ceria (SDC)*

Cerium(IV) oxide (or, ceria—$CeO_{2-\delta}$) has a cubic fluorite structure, capable of large oxygen non-stoichiometry (δ) via oxygen vacancies. In the moderate oxygen partial pressure atmospheres experienced by the SOFC electrolyte (known as the electrolytic regime), the oxygen vacancy concentration in ceria is extrinsically pinned down by a

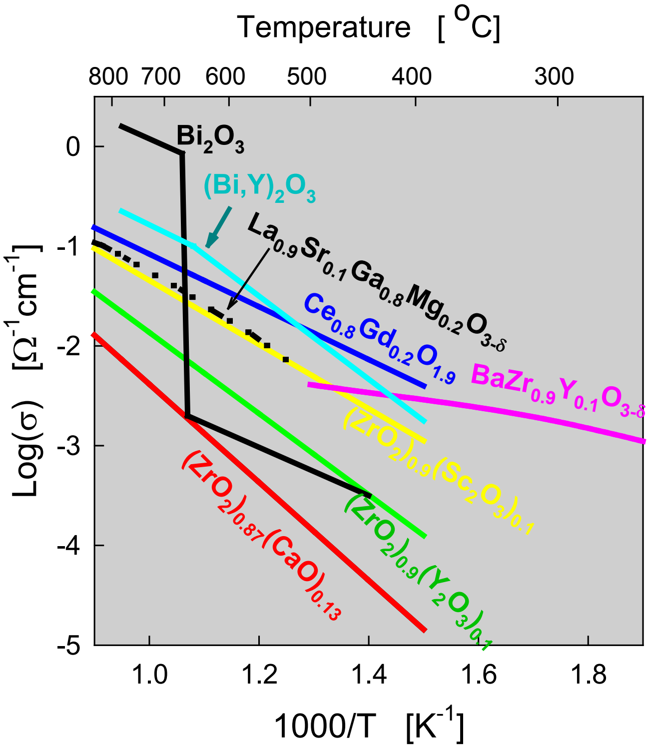

Fig. 1.3. A through-plane ionic conductivity comparison for common electrolyte materials taken from [13].

strictly 3+ cation dopant, such as samarium (SDC) or gadolinium (GDC). A samarium doping example is written here in Kröger-Vink notation:

$$Sm_2O_3 + 2Ce_{Ce}^{X} + 4O_{O}^{X} \leftrightarrow 2Sm'_{Ce} + V_{O}^{\cdot\cdot} + 3O_{O}^{X} + 2CeO_2 \qquad (1.5)$$

This induces significant ionic conductivity at intermediate temperatures, garnering much interest for doped ceria as the SOFC electrolyte component [15-17]. Fig. 1.3 shows a conductivity comparison between common SOFC electrolyte materials, including the traditional favorite, yttria-stabilized zirconia (YSZ)[14]. A generally accepted benchmark for electrolyte conductivity is ~0.01 S cm^{-1}, above which a candidate is deemed suitable. According to this metric, ceria-based electrolytes could potentially operate from 500 – 650 °C, without sacrificing performance, as would be the case with YSZ.

Additionally, under the high temperature reducing conditions typically seen in a SOFC anode, intrinsic oxygen vacancies form spontaneously via the oxidation of lattice oxygen, according to [1]:

$$O_O^X \leftrightarrow \tfrac{1}{2}O_2(g) + V_O^{\cdot\cdot} + 2e' \qquad (1.6)$$

These vacancies are charge compensated by electrons, which subsequently cause the cerium cations to change valence from nominally all 4+ to mixed 4+/3+. This gives rise to a non-trivial electronic conductivity via polaron hopping, making ceria a so-called mixed ionic-electronic conductor (MIEC). Although MIEC perovskite-type metal oxides are commonly employed as cathodes [18-20], there are few that are stable under the anode's high temperature reducing conditions, and those that are have low conduction and/or slow hydrogen electrooxidation kinetics [21-23].

Due to the lack of available MIECs, a traditional SOFC anode is typically composed of a random, three-dimensional amalgamation of an electronically conducting phase, e.g., nickel, an ionically conducting phase, e.g., YSZ, and a gas-permeable "phase," e.g., a network of pores [24-25]. The intersection of these three phases is termed the three phase boundary (3PB), shown schematically in Fig. 1.4a. The 3PB density (Fig. 1.4b) defines the number of reaction sites per projected electrolyte area, as the anode half-reactions can only take place at this intersection. This is in stark contrast to a MIEC, where electrochemical reactions can theoretically take place at nearly any point along its exposed surface, or the two phase boundary (2PB), as in Fig. 1.4c. There has been a significant effort to establish and quantify the anodic electrochemical activity of ceria-based 2PBs, even in the absence of a closely-adjacent, purely electronically conducting phase [26-32]. Therein, it is definitively shown that the surface of doped ceria alone is,

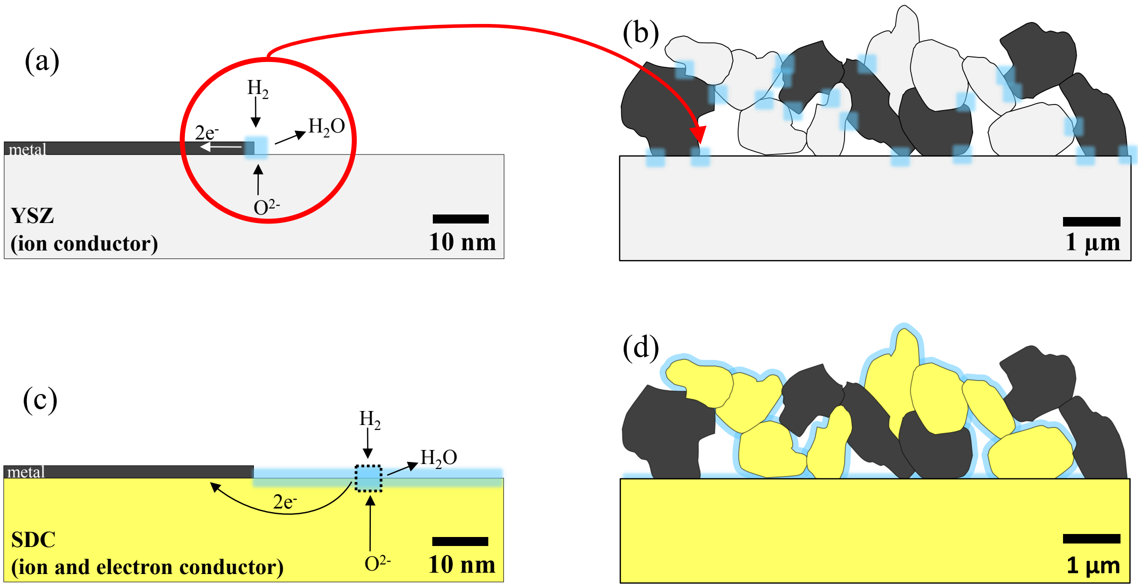

Fig. 1.4. Schematic diagrams of (a) the three-phase boundary (3PB) region where gas, metal, and yttria-stabilized zirconia (YSZ) phases intersect; (b) the 3PB density for a powder-processed anode; (c) the two-phase boundary (2PB) region of a mixed ionic-electronic conductor like samaria-doped ceria (SDC); and (d) the 2PB density for the same anode as in (b), but with SDC instead of YSZ. Light blue areas indicate electrochemically active regions.

itself, electrocatalytically active, and its bulk electronic conductivity is sufficient to place a current collector up to several microns away from a reaction site. Comparing the visualized anodes in Fig. 1.4b and d, it can be seen that a simple materials switch from YSZ to SDC affords a much greater reaction site density, owing to 2PB dominance over 3PB. In this way, materials selection paves the way for an architectural design paradigm, one where 2PB microstructures, rather than more restrictive 3PB microstructures, are possible.

1.2.3 *Cell Architecture*

Returning to the polarization curve of Fig. 1.2, there are three general design guidelines related to the three overpotentials outlined above. First, to reduce ohmic losses, all conduction pathways should be kept as short as possible. The primary culprit of ohmic loss is oxygen ion transport through the solid electrolyte—the conclusion here is simple: make the electrolyte layer thin (μm scale). Second, for a given electrode reaction rate, maximizing the number of active reaction sites will increase the current density, on the basis of the projected area of the cell. For a MIEC anode like SDC, this effectively translates into maximizing the active surface area (nm scale). Third, one must ensure easy gas phase access by highly porous, non-tortuous electrodes, although this is less of a concern than the previous two (μm and perhaps nm scale).

The ideal cell design must balance μm and nm length scales, which also means that new fabrication approaches must accommodate both. As SOFCs are high temperature devices, care should be taken to ensure stability of any as-fabricated nanometer-sized features. Despite the obvious need for feature size reduction, a general hierarchical structure is desirable for aspects like electronic current collection—electrons cannot be expected to only travel through nanometer-sized metal films or multiple-micron-lengths of SDC without incurring severe resistance penalties.

State-of-the-art powder processing methods that produce Ni/YSZ cermet anodes (as in Fig. 1.4b) are cheap and scalable, but offer limited structural tunability and little fundamental insight into the details of SOFC operation [25]. This is primarily due to the randomized nature of the electrode geometry—key features like 3PB (or 2PB in the case of a MIEC), pore size, conduction pathway lengths, and so on are all ill-defined. Even if these parameters are determined post production (and probably using a destructive method), the sample-to-sample variation is relatively high for randomized structures [33]. On the other hand, cell architectures with specifically engineered and well-defined geometries offer dual advantages of physically-correlated diagnostic analyses and the subsequent ability to alter the design in accordance with the results. For instance, knowing the relationship between a SDC anode's 2PB and its impedance spectra (c.f. Chapter 4) could lend valuable insight into which design knob to turn, and how much.

In summary, most operational voltage loss mechanisms in today's SOFCs inform an overall feature size reduction of every component of the cell architecture. This move should be done intelligently, so as not to incidentally incur other penalties, e.g., gas diffusion limitations and bulk transport resistances, while at the same time maintaining manufacturability, scalability, and the ability to produce large total footprint cells. Furthermore, trending towards defined, as opposed to randomized, geometries can help link performance to tunable features.

As such, there is tremendous need and potential for entirely new SOFC design schemata, as well as complimentary fabrication techniques.

1.3 Anti-Dot Substrates: A New Design Framework

In recognition of the need to examine geometrically well-defined structures, some recent mechanistic studies have employed two-dimensional electrodes patterned onto the electrolyte of interest [18, 34-36]. This approach has begun to bear fruit and mechanistic models have begun to be developed [37-38]; however, challenges in understanding 'real' fuel cells remain because the two-dimensional patterns have a substantially lower areal density of 3PBs (defined as the 3PB length per unit of projected electrolyte area) than the systems they represent. Specifically, conventional photolithographic techniques with a minimum feature size of about 5 μm can attain a maximum areal 3PB density of 2,000 cm cm^{-2} [34]. In contrast, typical fuel cell electrodes boast values as high as 800,000 cm cm^{-2} [33]. Such significant microstructural differences can plausibly induce differences in reaction pathways. Accordingly, there is a pressing need to obtain geometrically defined electrode structures with tunable feature sizes that are more relevant to SOFC electrocatalysis.

Demonstrated below is a facile fabrication strategy, known as polymer sphere lithography, in which monodisperse polymer spheres serve as sacrificial templates to construct anti-dot metal films (see Fig. 1.5a), permitting access to 3PB areal densities over an enormous range, from 2,000 to 43,500 cm cm^{-2}. Though not previously explored in the fuel cell context, the anti-dot structure is ideal for advancing the aforementioned fundamental studies for this reason.

When these porous, metal films are overlaid onto an electrolyte substrate such as YSZ or SDC, the fraction of exposed electrolyte area and the 3PB are concurrently and specifically known, true for all two-dimensional lithographic processes. This enables electrocatalysis studies for the underlying electrolyte material, particularly as it pertains to 3PBs (and 2PBs for MIECs). The accessible 3PB regime here is previously untouched by conventional lithography, moving much closer to actually-in-use 3PB densities. Use in conjunction with diagnostic tools such as A.C. Impedance Spectroscopy (ACIS) allows definitive relationships between 3PBs/2PBs and various electrochemical activity-related materials characterization parameters to be established, e.g. rate limiting processes' resistances, capacitances, etc. And when combined with traditional lithography techniques, an extremely wide range of 3PBs can be sampled. Although tempting, such a geometry as-is, however, is not actually a suitable electrode candidate because of issues like high electronic resistance through the relatively thin anti-dot metal film.

An even higher number of reaction sites can be achieved by moving from a planar to a three-dimensional structure, and these anti-dot films are a good starting point to get a variety of well-defined three-dimensional electrode structures.

Chapters 2 and 5 present the fabrication of the anti-dot structure and its derivatives, and Chapter 4 discusses the performance of its related SOFC electrodes.

1.4 Three-Dimensional Structures and Their Fabrication by CELD

Using the anti-dot structure as a starting point for the fabrication of high surface area three-dimensional structures, several specific, more optimized architectures can be considered, as in Fig. 1.5. Cathodic electrochemical deposition (CELD) is an ideal candidate to produce template-free high surface area structures, as well as templated frameworks like inverse opals (Fig. 1.5c and d) and nanowires/tubes (Fig. 1.5e). As a testimony to their flexibility, anti-dot based substrates can also accommodate new and old approaches such as screen printing [39], pulsed-laser deposition (PLD) [40], chemical vapor deposition (CVD) [41], and CELD (c.f. Chapter 3).

1.4.1 *SOFC Fabrication Method/Morphology Non-Negotiables*

Up to this point, only general SOFC materials/architectural design guidelines have been discussed, without reference to a particular method to produce such schemes. This section is devoted to the assessment of new fabrication techniques and their associated as-produced morphologies, to aid in their development.

Before any new fabrication method/morphology is adopted for SOFCs, a few non-negotiable requirements must be met. First, the fabrication method must be able to

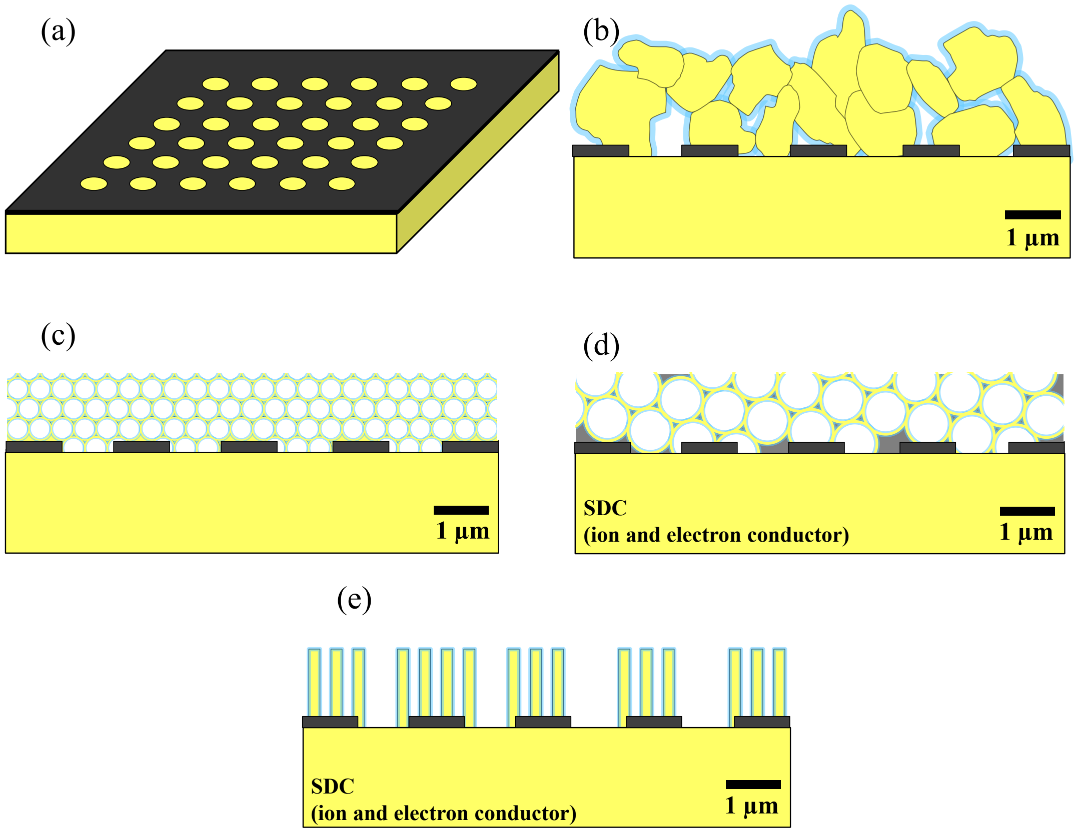

Fig. 1.5. (a) A schematic of a metal anti-dot network; (b) a cross-sectional depiction of the anti-dot film in (a) replacing metal powder as a current collector and thereby increasing the 2PB density; and examples of potential templated electrodes with tunable geometries like inverse opals (c) and (d), and nanowires (e).

consistently produce the desired materials composition. Keeping large-scale manufacturability in mind, basic repeatability is absolutely necessary. Second, the as-deposited morphology/microstructure cannot be adversely affected by SOFC operating conditions, e.g., high temperatures, oxidizing/reducing atmospheres, etc. This includes, for instance, cracking in electrolytes and agglomeration of small features in electrodes. Third, continuous and accessible migration pathways to and from surface reaction sites must exist in the electrodes. Of course, low resistance pathways are desirable, rather than only connected ones.

In this manuscript, cathodic electrochemical deposition is evaluated as a components fabrication tool for a SDC-based, intermediate temperature SOFC.

1.4.2 *Cathodic Electrochemical Deposition (CELD)*

CELD is a liquid-based, low temperature fabrication technique that is able to produce ubiquitous and conformal metal oxide/hydroxide coatings of tunable surface area at low capital and operational costs [42-43]. The experimental setup is straightforward (see Fig. 3.2): three electrodes are immersed in a liquid electrolyte—electrons flow out of the anode and into the cathode through the external circuit, and the reference electrode measures the cell potential but does not allow any current to flow through it. A working potential is applied, and the appropriate electrochemical reactions occur.

Being liquid-based makes CELD scalable as a batch process, and allows easy control of large substrates, even if irregularly shaped: appropriate operating configurations ensure uniform deposition on protruding and porous substrates alike. Furthermore, cation doping in liquid systems is simple [44-47], while the low operating temperatures diminishes the incorporation of undesirable impurities. Low temperatures and open, ambient conditions also reduce the experimental complexity, especially in regard to otherwise stringent substrate requirements. Other common metal oxide fabrication methods, such as CVD and PLD, typically involve *in situ* high temperatures with a background atmosphere of oxygen—prime conditions for unwanted oxidation of metallic substrate components, and risky due to the potential for impurity incorporation into the oxide phase. CELD is also favorable as a manufacturing process as deposition times are on the order of minutes, rather than hours or days. In addition to being explored for general SOFC applications [48-52], CELD ceria has been previously studied for corrosion protective coatings [46, 53-56], superconductor buffer layers [44], powder synthesis for increased sinterability [57], and nanowire/tube fabrication [49, 58-59]. Aside from ceria, other SOFC-relevant materials have been produced using this method, such as $BaTiO_3$, Nb_2O_5, ZrO_2, $LaMnO_3$ [42], and Y_2O_3 [60].

There are two general categories of oxide/hydroxide electrochemical deposition, defined by which electrode experiences the desired deposition, known as the working electrode. Anodic electrochemical deposition (AELD) directly oxidizes $Ce^{3+}(aq)$ ions to insoluble Ce(IV) [54, 61-62]. A stabilizing ligand must be added to the electrolyte solution to ensure that Ce(III) species do not precipitate prematurely. A fundamental limitation of this technique is that Ce^{3+} ions must contact a surface that can conduct electrons away; as CeO_2 is generally insulating, AELD should only be able to deposit extremely thin films, on the order of tens of nanometers.

Cathodic electrochemical deposition, on the other hand, proceeds by a two-step process. First, the electrolyte solution becomes progressively basic as electrochemical reduction reactions of various electrolytic species occur due to the applied cathodic potential at the cathode|electrolyte interface. This is widely referred to as electrogeneration of base. Second, the newly-formed base induces chemical precipitation of Ce(III/IV) species, e.g. $Ce(OH)_3$ or hydrated CeO_2, which are finally oxidized to the desired fluorite CeO_2 phase. It is somewhat surprising that a Ce(IV) deposit on the cathode could result from a nominally Ce^{3+} electrolyte—this is a testament to the purely chemical nature of the deposition step. Restated, the nucleation and growth process here is non-Faradaic. One example reaction each from the electrogeneration of base and precipitation steps is given in Eqns. (1.7) and (1.8), respectively, although a myriad of possibilities exist (see Chapter 3 for an in-depth discussion).

$$O_2 + 2H_2O + 4e^- \rightarrow 4OH^- \tag{1.7}$$

$$Ce^{3+} + 3OH^- \rightarrow Ce(OH)_3 \tag{1.8}$$

Detailed investigation of and results from the CELD of ceria microstructures are presented in Chapters 3 and 5. Performance analyses of CELD ceria-based SOFC anode structures are presented in Chapter 4.